NASA Technical Paper 1209

Remote Sensing of Gulf Stream Using GEOS-3 Radar Altimeter

Clifford D. Leitao, Norden E. Huang,
and Carlos G. Parra

APRIL 1978

NASA

NASA Technical Paper 1209

Remote Sensing of Gulf Stream Using GEOS-3 Radar Altimeter

Clifford D. Leitao and Norden E. Huang
Wallops Flight Center
Wallops Island, Virginia

Carlos G. Parra
EG&G Washington Analytical Services Center, Inc.
Pocomoke City, Maryland

National Aeronautics
and Space Administration

**Scientific and Technical
Information Office**

1978

REMOTE SENSING OF GULF STREAM USING GEOS-3 RADAR ALTIMETER

by

Clifford D. Leitao
Norden E. Huang
NASA Wallops Flight Center

and

Carlos G. Parra
EG&G Washington Analytical Services Center, Inc.

INTRODUCTION

The study of the general ocean circulation has long occupied the central stage of physical oceanography and the most important phenomena in the ocean circulation investigations are the major boundary current systems such as the Gulf Stream and Kuroshio. For the Gulf Stream, most of the results from past studies have been summarized by Stommel (ref. 1) in a classical work. Although the results are voluminous, our knowledge of the global ocean circulation in general and the Gulf Stream in particular is still quite limited. The main difficulties arise from the methods of observation. Even though major improvements have been introduced over the last two decades or so in the observational methods such as the geomagnetic electro kinetograph method (ref. 2, 3); remote tracking capability of neutrally buoyant floats (ref. 4) and surface buoys (ref. 5); bottom moored current meters (ref. 6) and improved CTD Systems, the most widely used method is still based on hydrographic data collected on various cruises by ships. Since large scale motions in the open ocean are essentially geostrophic, the value of those hydrographic data is undisputable in understanding the mean and other statistical characteristics of phenomena with scales such as that of the Gulf Stream as demonstrated by Worthington (ref. 7) and Dantzler (ref 8). But burdened by the detailed data collection procedures and the slow speed of the ships, the data have never been synoptic even with multiple ship deployment as reported by Fuglister (ref. 9, 10).

The difficulty of lacking synoptic coverage has been alleviated by the introduction, a few years ago, of surface IR data collected from satellites. The potential of these data is clearly demonstrated in a series of papers by Warnecke et al. (ref. 11), Rao et al. (ref. 12), Strong and DeRycke (ref. 13), Richardson et al. (ref. 14), DeRycke and Rao

(ref. 15), Legeckis (ref. 16), Stumpf and Rao (ref. 17) and Voorhis et al. (ref. 18). Enlightening as they are, there are some intrinsic technical weaknesses that limit the usefulness of this important data source as discussed by Clark (ref. 19), LaViolette and Chabot (ref. 20), Maul and Sidran (ref. 21) and McGrath and Osborne (ref. 22). Aside from those technical difficulties, even under ideal conditions the IR data can only be used to delineate the surface boundaries of water masses having strong thermal gradients (ref. 23). On the crucial dynamic parameters such as the location of the Gulf Stream axis and the magnitude and distribution of the velocity along the axis, the information from the IR data is nil.

Recently, the development of an accurate radar altimeter operational under all weather conditions has reached a new level of success. Direct measurement of the sea surface topography with an accuracy of ±20 cm for one second averaging from a stable moving reference platform provided by a satellite is now possible. This offers a direct way to measure the dynamic topography which until now could only be inferred from hydrographic data. From the altimeter data, the surface current can be calculated directly from the surface slope using the geostrophic equation (ref. 24). In this paper, the basic principle of altimetry is reviewed for the sake of completeness; then some recent results are presented. Finally, the potential and the weakness of altimetry applications in future oceanographic studies are briefly discussed.

SATELLITE RADAR ALTIMETER

A satellite radar altimeter is a high precision instrument capable of accurately measuring the distance between the satellite platform and the sea or ground surface. The principle of radar altimetry was first proposed by Godbey (ref. 25); Frey et al., (ref. 26) discussed the detection of sea surface dynamic topography using a radar altimeter and, Greenwood et al. (ref. 27) addressed the applications of the altimeter to physical oceanography. Recently, McGoogan (ref. 28) discussed the principles on a wider scope including applications to both sea surface height and sea state studies, and provided specific details on the feasibility of the proposed applications using actual data from the Skylab radar altimeter. Although the principles involved in sea surface height measurement are simple, the practical difficulties are many. The measurements made by a satellite altimeter are illustrated by Fig. 1. An ideal altimeter will yield measurements on satellite altitude which may be expressed as:

$$h_a = h_s - h_g - \Delta h \ , \qquad (1)$$

where h_a is the satellite altitude measured by the altimeter, h_s is the satellite height

above a reference spheroid determined from the satellite tracking data, h_g is the geoidal deviation from the spheroid due to gravitational anomalies and Δh is the height deviation from the geoid due to the dynamic processes in the ocean such as the currents and tides.

In the ocean, the value of h_g can be as high as two orders of magnitude larger than Δh (ref. 26). Consequently there are two prerequisites for applications of altimetry to ocean dynamics; namely, high altimeter resolution and precision so that Δh will be discernible above the strong dominant signal of h_g, and detailed knowledge of the geoid so that h_g can be properly subtracted without introducing aliasing in Δh. At present, knowledge of a global geoid based on available geophysical data is far from being adequate (ref. 29); and prior to GEOS-3 the altimeter was not accurate enough (ref. 30). This essentially limited the early applications of the altimeter to the study of the marine geoid as reported by Leitao and McGoogan (ref. 31). An attempt to extract ocean dynamic signals by Leitao et al. (ref. 32) was not conclusive. The situation is now changed by the successful launching of the GEOS-3 satellite.

To achieve maximum flexibility and to preserve power, the GEOS-3 altimeter was designed to operate in two modes: global and intensive, both operating at a frequency of 13.9 Ghz. In the intensive mode a pulse compression technique produces a 12.5 nsec pulse width and provides measurements with an accuracy of ±20 cm over a one second average. This configuration gives a footprint size of 3.6 km wide and 11 km along the track from an orbit height of 840 km with zero eccentricity. A detailed technical discussion of the GEOS-3 radar altimeter is given by Hofmeister et al. (ref. 33). The orbit has an inclination angle of 115°, so successive tracks will cross the equator every 101.8 minutes with a precession of about 26°. Thus for any given region the satellite will cover a 1° x 1° grid in approximately one month. Since no data memory is available aboard the satellite, altimeter data acquisition is limited to areas where telemetry stations are located.

In order to accurately calculate the distance, knowledge of the orbit and the pointing angle is essential. The attitude of the satellite is stabilized with a special subsystem which incorporates a gravity gradient boom, boom end mass and damper, augmented by a constant speed angular momentum wheel; thus maintaining the satellite within ±0.5° of nadir pointing 98% of the time. The satellite is also accurately tracked by using both C-Band and S-Band radars, and laser systems to achieve ±5 m accuracy in height above the spheroid, and ±10 m and ±50 m in along and cross-track orbit positioning respectively. The large amount of uncertainty in the along-track and cross-track orbit position is not a serious limitation to ocean dynamics applications since these perturbations are usually of much longer wavelength on the order of 10^6 - 10^7 m (ref. 34, pp. 317-334); than any ocean dynamic signature discussed here. It may, however, cause considerable difficulty in geodesy (ref. 35). A 5' x 5' detailed gravimetric geoid was computed by Marsh and Vincent (ref. 36) covering an area from 16°N to 39°N latitude and 60°W to 82°W longitude. The geoid computation technique uses mean surface gravity data to compute the short wavelength

contribution to the geoid, and each mean anomaly is weighted solely as a function of its distance from the computation point. However, different methods used to compute the mean gravity anomalies, because of the type or lack of point anomaly gravity data, can produce a heterogeneous data base which is not accounted for in the geoid computation. Also, the distribution of point anomaly data is dense in some areas and sparse or nonexistent in others. This results in a difference in the standard deviation of the mean anomalies, which also is not accounted for in the geoid computation. Finally, the point anomaly sampling in areas where large gravity anomalies exist has to be dense and well distributed to provide meaningful mean anomaly data for the geoid computation. Results where the above problems occur off Cape Hatteras and the South Atlantic Bight are discussed below. In most areas northeast of Hatteras the geoid is known well enough to make the study of Gulf Stream dynamics feasible. This geoid was improved upon by Marsh and Chang (ref. 37) and scaled down 5 m to account for the difference in semi-major axis, and is used as the reference geoid in this work.

DATA PROCESSING

The GEOS-3 satellite was launched on April 9, 1975. The first few months were devoted to launching and operational assessment, and experiment system calibration and evaluation. Intensive coverage of the Gulf Stream area started in late July, 1975. Data from most of the intensive mode, northbound passes collected in the months of August, September and October 1975 are presented here.

The altimeter is designed to make 100 individual measurements per second and to either telemeter them or a 10 pulse per second average to the telemetry stations (ref. 33). In order to eliminate some internal random noise and to save data processing time, only the 10-pulses per second averaged data are used. The averaged altimeter measurements are then preprocessed and converted to sea surface heights (ref. 38) and are treated here as raw sea surface heights. The data processing procedure is summarized in Fig. 2, using data from orbit 1710. The raw sea surface heights shown in Fig. 2A are first edited to eliminate anomalies due to internal instrument noise. The edit criterion is based on a predicted sea surface height calculated by fitting a straight line through the last eight seconds of data (80 data points representing 60 km in physical distance). Any point differing from the predicted height by more than two meters (approximately three standard deviations of the noise level of 70 cm) is replaced by the calculated predicted height value. The edited sea surface height data shown in Fig. 2B is then filtered using an 81 point, equal-weight, mid-point filter. This filter is chosen since it reduces the noise without seriously compromising the sea surface signature. The eight seconds were selected

so that the accuracy could be maintained below the 10 cm level; and the noise level is sufficiently reduced prior to differentiation. After the filtering process, the smoothed sea surface height is referenced to the Marsh-Chang (ref.17) 5' x 5'geoid (see Fig. 2C). Subtracting the geoid from the smooth sea surface height results in a residual which is nearly flat in the open ocean, as shown in Fig. 2D. Next, to minimize the error between the geoid and the smooth sea surface height south or east of the mean position of the Gulf Stream, a linear fit is made to the residuals over the section representing the open ocean and encompassing approximately the first 100 seconds of data. The straight line is then subtracted from all the residuals, thus removing any potential orbital bias or slope errors and producing an estimate of dynamic heights, as shown in Fig. 2E. Finally, the dynamic heights are differentiated with a filter designed to match the smoothing filter in order to compute the slope of the sea surface. The slope is substituted in the geostrophic equation to obtain velocity measurements as shown in Fig. 2F.

RESULTS

The coverage of northbound GEOS-3 altimeter data over the East Coast of the United States during August, September and October 1975 used in this study is shown in Fig. 3. Orbit numbers and dates are shown in Table I. However, the quality of the results vary over this area depending on the accuracy of the geoid. The region near Cape Hatteras gives the most trouble primarily because of the lack of accurate, well distributed gravity data and because the Gulf Stream flows over the sharpest change in bottom topography. Consequently the largest geoid change coincides with the dynamic topographical adjustment due to the Gulf Stream, making the identification of the Gulf Stream signal difficult at present. For the region south of the North Carolina capes, the same problem still exists but to a lesser degree, and other difficulties also arise. The inner continental shelf in the South Atlantic Bight lies on the Blake Plateau which rises to less than 1000 m from the ocean basin floor. As a result, the Gulf Stream in this region generally flows over the relatively shallow plateau water hugging the inner continental shelf. Thus, the influence of the submarine topography becomes an important parameter in the dynamics of motion as indicated by the existence of topographically induced eddies observed by satellite IR data (ref. 16). Also, due to local meteorological conditions and instability of Gulf Stream flow, numerous incidences of shelf water entrainment occur (ref. 39-41); additional small scale eddy spin-offs are also very common (ref. 42). Because of the relative shallowness of the water over this region and the complicated interactions of shelf water and the Gulf Stream, the simple geostrophic assumptions may not be sufficient to fully explain the flow pattern. Furthermore, due to the low surface thermal gradient between

the Gulf Stream and relatively warm ambient water and due to persistent cloud cover (see NOAA's Experimental Gulf Stream Analysis charts for August, September, and October 1975), satellite IR imagery is not usable most of the time for this experiment. This eliminates an important collaborating data source which is quite necessary at this stage of research. Therefore, results for near Cape Hatteras and for the South Atlantic Bight will not be utilized.

Northeast of Cape Hatteras, the Gulf Stream leaves the continental margin and flows through a region that is about 4000-5000 m deep where geoid changes are gradual and well defined. Since the high velocity core of the Gulf Stream usually does not penetrate much below 1500 m (ref. 1), the influence of bottom topography is negligible except possibly near isolated seamounts. Therefore results over this region are examined in detail and presented as follows:

The Position of the Gulf Stream

A comparison is made between the positions of the western boundary of the Gulf Stream as determined by the altimeter data and the results of the chart of the Experimental Ocean Frontal Analysis (EOFA) published weekly by the Naval Oceanographic Office and chosen to best approximate the pass time and date. The Gulf Stream boundaries determined from the altimeter data are defined at the breaks of the sharp height changes. The boundaries of the stream can also be determined from the EOFA charts which are based on data from VHRR-IR of the NOAA-4 satellite, sea surface temperature measurements from injection temperature by surface ships, ocean weather ships, and Coast Guard monthly IR survey flights (see Fig. 4). From this comparison, the discrepancy in the location of the western boundary can be measured and the result is presented in Fig. 5. The bias of the altimeter-determined western boundary is 23 km ± 36 km west or north of the highest thermal gradient at the surface.

It is interesting to compare the present result with that of Hansen and Maul (ref. 23) who compared the location of the Gulf Stream axis at the position of the 15°C isotherm at 200 m depth with the maximum surface temperature gradient. Since the maximum surface temperature gradient is usually treated as the boundary of the Gulf Stream, it is logical that the surface boundary should have a westward or northward bias from the axis. The discrepancy was found to be 14.5 ± 11.8 km. However there may be some question with regard to the definition of the stream boundary at the surface using the maximum temperature gradient. The temperature signature is undoubtedly a good indicator for water mass, therefore the line may indeed offer the demarcation between the Gulf Stream and ambient waters. But the finite phenomenological eddy viscosity for the Gulf Stream system with a magnitude in the order of 10^6 cm^2/sec (ref. 43) clearly requires a momentum transition

zone. Consequently, the velocity field may be much wider than indicated by the water mass boundary thus resulting in a farther westward or northward shift. This argument can be supported by other considerations. First, if the maximum surface temperature gradient line were indeed the boundary, then the discrepancy between this line and the 15°C-200 m location will be on the order of half the width of the stream. A 14.5 km mean half width is obviously too small a mean value even assuming an asymmetrical distribution of Gulf Stream velocities. Also, the present result shows an additional shift of 23 km, that will mark the half width on the order of 40 km, which is much more reasonable. Second, the hydrographic section data (ref. 10) also indicated additional vertical density structures outside the maximum thermal gradient zone which produce the necessary balance of force to support a current at the surface layer outside the maximum surface temperature line. Finally, the filter length could also cause bias in the definition of the Gulf Stream boundary, which will be discussed later.

A few remarks are offered here to explain the large standard deviation of the discrepancy. Most of the discrepancy occurs when the location of the Gulf Stream on the EOFA chart is shown by dashed lines, indicative of a lack of data due to cloud cover or a lack of sufficient ship reports. Due to weather conditions, this uncertainty can be extensive both in time and space. For example, extensive cloud cover over most of the study area lasted from mid-August through the beginning of September spanning more than three weeks. This added considerably to the large discrepancy. Hindcast analysis using all the data would undoubtedly reduce the scatter.

The Mean Velocity Distribution

The mean velocity values are then calculated from the dynamic heights as an estimate of the speed of the Stream. The calculations were based on the simplified geostrophic equation:

$$V_o = \frac{g}{2\Omega \sin\phi} \frac{\Delta h}{\Delta L \sin\theta} , \qquad (2)$$

where V_o is the surface velocity; g is the gravity acceleration at 980 cm/sec^2; Ω the angular speed of the earth; ϕ, the latitude of the location; Δh, the total height anomaly; ΔL, the horizontal distance over which the height anomaly occurred; and θ, the angle between the sub-satellite track and the axis of the Gulf Stream. The term involving θ is necessary since the subsatellite tracks are not always perpendicular to the axis of the Stream. The value of θ is determined from the EOFA charts. The mean velocity values calculated through this process are presented in Fig. 6. These velocities are produced by a slope calculation based on the total height difference across the Gulf Stream and

are therefore an average value smaller than results shown in the next section. The overall mean velocity (total height difference/total width) of the tracks processed is 107 cm/sec with a standard deviation of 29 cm/sec. These values are certainly within the ranges of observations summarized by Stommel (ref. 1). When the observations by NOAA satellite are hindered by extensive cloud coverage, the angle cannot be accurately determined. This difficulty can be overcome in the future by another method of data processing which will be discussed later.

Comparison of Velocity Profiles of Repeated Passes

In the region northeast of Cape Hatteras, there are two locations where three sub-satellite tracks come within 5 km of each other. A detailed comparison of these passes will reveal not only the time history of the Gulf Stream, but also will provide an internal check on the consistency of the data. The first set includes orbits 1795, 2321 and 2847 and the second set consists of orbits 1710, 2236 and 2762. The dynamic topography and the velocity profiles are presented in Figs. 7 and 8. The similarities of the topographic features are striking especially toward the open ocean. They could be caused by geoid changes, however their time variability makes it highly unlikely. But these small uncertainties do not seriously compromise the Gulf Stream signature. The location of the Gulf Stream does not undergo considerable change, which is independently supported by the EOFA charts. Yet there is a systematic spatial change over the three month period. Although only two sets of data are available, the decreasing maximum velocity trend is similar to the mean values reported by Fuglister (ref. 44) for the months of August, September and October in the region northeast of Hatteras. A striking dynamic implication can be drawn from the profiles i.e., the Gulf Stream seems to be consisting of branches of flow rather than a single coherent stream or jet. This is similar to one of the interpretations (ref. 9) from the multiple ship data where the Gulf Stream was regarded as consisting of a "turbulent confusion of disconnected fragments" (ref. 1, p. 74). The amplitude of the fluctuations increase as the Stream moves downstream which is consistent with the meander characteristic reported by Hansen (ref. 45). This magnitude of the surface height fluctuations (1 m) indicates that velocities over 100 cm/sec are possible. Some of the fluctuations may appear in the form of eddies or rings (ref. 14, 46), but the possibility of fragmentary flow patterns cannot be ruled out. The existence of such energetics near the major boundary current is suggested by Wyrtki et al. (ref. 47). Recent data of long-term moored current meters from MODE (ref. 48-50) seem to corroborate the findings. While complete understanding of the interactions of the eddies and large-scale circulation is yet to come, it is hoped that future observations such as the POLYMODE experiments will resolve some of the questions.

The Dynamic Topographic Maps

Dynamic topographic maps provide a wealth of information about the dynamics of ocean circulation. However they are costly to obtain through conventional hydrographic methods. Since altimetry provides a direct measurement of the height of the ocean surface, a topographic map can be produced directly from the composite results from several orbits. Monthly dynamic surfaces using the dynamic heights at intervals of 20 cm for the months of August, September, and October are presented in Figs. 9, 10 and 11. The direction, number, and both time and spatial distribution of the satellite passes influence the validity of each map to a large degree. It must be pointed out that these maps are not monthly averages but rather a mosaic consisting of instantaneous measurements obtained at different times during the month similar to a scanning time exposure along the sub-satellite tracks. When the data are not of sufficient density, dashed lines are used for contours.

Information on the location and intensity of the Gulf Stream and other dynamic features can be deduced from these maps. The current can be recognized to be located at the steepest slopes above 35°N. Its location and magnitude is similar to the annual mean sea surface topography (ref. 51). The Gulf Stream boundaries inferred from these maps agree rather well with the EOFA analysis except for orbit 1923 which is at the end of an intensive cloud cover period.

In analyzing the maps, both static and dynamic features are observed. For example, at 38°N, 72°W a depression in the ocean surface is shown in all three maps. This feature seems to be caused by a poorly defined geoid in that area since it does not change with time and it occurs close to the 200 m isobath. The maximum latitude covered by the geoid (39°N) precludes any analysis above that latitude; therefore, very few anomalies in the sea surface associated with warm eddies are encountered. The propagation of meanders (ref. 44) can be seen in the maps for the months of August, September and October. The incipient meander seen at 37°N, 71°W in orbit 1852 in August has moved more than 300 kilometers to about 37°N, 68°W in orbit 2122 in September and it has intensified by October in orbit 2648. However, because of the time difference among the tracks, some problems arise. For example, the two sharp bends around orbits 2435 and 2122 may also be attributed to changes in time and space. For orbit 2435, the two neighboring tracks are 2236 and 2108. The dates of data collection for these orbits are September 29, 15, and 5 respectively which represents a large time separation; for orbit 2122, 2321, and 2449, the dates are September 6, 21, and 30 an even worse time separation. This discrepancy can be alleviated with the incorporation of southbound orbits, then the data density will be doubled or the time required to produce the same contour map can be reduced to 15 days, which is approximately the time scale for meanders in this region (ref. 51).

Associated with this space-time problem is the movement of eddies. If an eddy is moving, the image on this scanning time exposure will be an elongated anomaly. This can

be seen on the map for August along 67°W, between 35° and 36° N where the elongated depression coincides with an eddy identified by surface temperature data. Depressions such as that positioned at about 33° N, 64° W in August, have the right dimensions and symmetry to be called cold eddies (ref. 53). Yet, the lack of a fine density grid coverage for the month of September in that area does not allow a time series comparison of such eddies. This time-density problem will be alleviated in the future by incorporating southbound passes into the analysis.

DISCUSSION

Having presented the results, a few points which may have important bearing on the potential and validity of altimetry in the study of ocean dynamics in general and for ocean currents in particular should be addressed.

As discussed above, the geoid provides the equipotential surface from which the dynamic deviation can be calculated. This may not be a serious problem in the open ocean where the geoid is relatively flat. At some special locations such as the regions near Cape Hatteras and in the South Atlantic Bight where the changes of depth amounts to a substantial portion of the total depth, the geoid signal is much larger than the ocean dynamic deviations and the geoid sometimes becomes a problem. This difficulty causes special complications for ocean dynamic applications because there exists genuine interactions between the bottom topography and the dynamics of the currents (ref. 1, 54-56). Furthermore, accurate gravity and bathymetric data needed to compute the geoid for areas with sharp changing bottom topography are not always available at the required sampling density. The difficulty can be illustrated by two sets of data: three repeated passes over the Blake Spur in the South Atlantic Bight and two near Cape Hatteras. The surface height anomalies together with the bottom topographic changes are presented in Figs. 12 and 13. The influence of the Spur can be clearly seen on the surface data. The existence of the surface height anomalies produced by the Spur have seriously compromised the linear fit. The high dynamic heights caused by the poorly modelled geoid near Cape Hatteras are also obvious; the height differences imply a narrow Gulf Stream (70 km). The EOFA charts show the Gulf Stream to be twice as wide as these results indicate, with a western boundary southwest of the estimated position and no countercurrent. Typical values of the Gulf Stream width tend to contradict the analysis in this region. Obviously, the improvement of the geoid becomes the most urgent part of this task.

The raw, intensive mode, altimeter data are quite noisy (RMS noise 70 cm). In order to extract any useful information at all, filter techniques have to be used. The 81 point filter employed in this study causes the resolution of height anomaly features to

deteriorate rapidly as the scales of the features decrease. For the Gulf Stream, this limitation is not severe, but it does cause the height anomaly to spread over the filter length and this may contribute to a bias in the boundary definition of the Gulf Stream. Using a shorter filter will reduce the bias, but will increase the noise in the height anomalies. As a check of internal consistency, the RMS values of the dynamic heights over the region of the straight line fit for all the tracks northeast of Cape Hatteras plotted as a function of their equatorial crossing are presented in Fig. 14. It can be seen that the RMS values show an increase toward the downstream locations. This trend is consistent with the increase in number of eddies formed by the meandering pattern of the Gulf Stream. Additionally, higher sea states associated with these downstream regions may also contribute to a higher RMS. The lower limit of the RMS values, which is a measure of the accuracy of the altimeter is below 10 cm as predicted by the formula:

$$S = \left[\frac{\sum(Z_n - \bar{Z})^2}{n-1}\right]^{1/2} \qquad (3)$$

This further confirms that the one meter fluctuations observed over the Gulf Stream are definitely valid signals, and that any signal larger than 20 cm is also above the noise level. This justifies the choice of the 20 cm contour interval for the dynamic topography maps.

There are environmental conditions that can induce systematic biases in the altimeter ranging such as atmospheric conditions and sea state (ref. 33, 57); however these biases can be corrected with appropriate data, which are not available at the present.

Since the altimeter is essentially a profiler, additional data are needed to correct the relative direction of the sub-satellite tracks so that the velocity can be calculated correctly as discussed above, but this limitation is only valid for the present method of data handling. When fully operational, data from a second family of orbits in an approximately orthogonal direction to the present set can be incorporated in determining the dynamic topography maps. Once the dynamic surface contour is available, the mean direction of the current can be determined and no angle θ will be needed to correct the measurements. The surface velocity determined in this way, however, depends critically on the geostrophic assumptions. In the open ocean there are non-geostrophic currents such as inertia currents, wind induced drift currents and even wave induced mass transport. When the balance of forces does not require surface topography change, the altimeter data would be of little use.

In summary, the results of the present analysis indicate that with the GEOS-3 radar altimeter it is possible to measure the dynamic topography and infer the surface velocity in the western boundary current systems, provided the local geoid is accurately known. Although the altimeter will prove to be an important tool in physical oceanographic

research, ancillary measurements such as surface temperature and hydrographic sections will still be needed since a multi-sensor approach is necessary to provide the information for understanding ocean dynamic processes.

TABLE I. ORBIT NUMBER AND DATE OF PASSES USED FOR THIS STUDY

August 1975		September 1975		October 1975	
Orbit No.	Date	Orbit No.	Date	Orbit No.	Date
1611	1	2051	1	2492	3
1625	2	2080	3	2506	4
1667	5	2094	4	2549	7
1682	6	2108	5	2563	8
1710	8	2122	6	2606	11
1724	9	2137	8	2620	12
1753	11	2151	9	2648	14
1781	13	2165	10	2677	16
1795	14	2179	10	2691	17
1810	15	2208	13	2705	18
1824	16	2236	15	2719	19
1838	17	2264	17	2748	21
1852	18	2307	20	2762	22
1881	20	2321	21	2790	24
1909	22	2336	22	2819	26
1923	23	2350	23	2847	28
1966	26	2392	26	2862	29
2037	31	2407	27	2876	30
		2421	28	2890	31
		2435	29		
		2449	30		

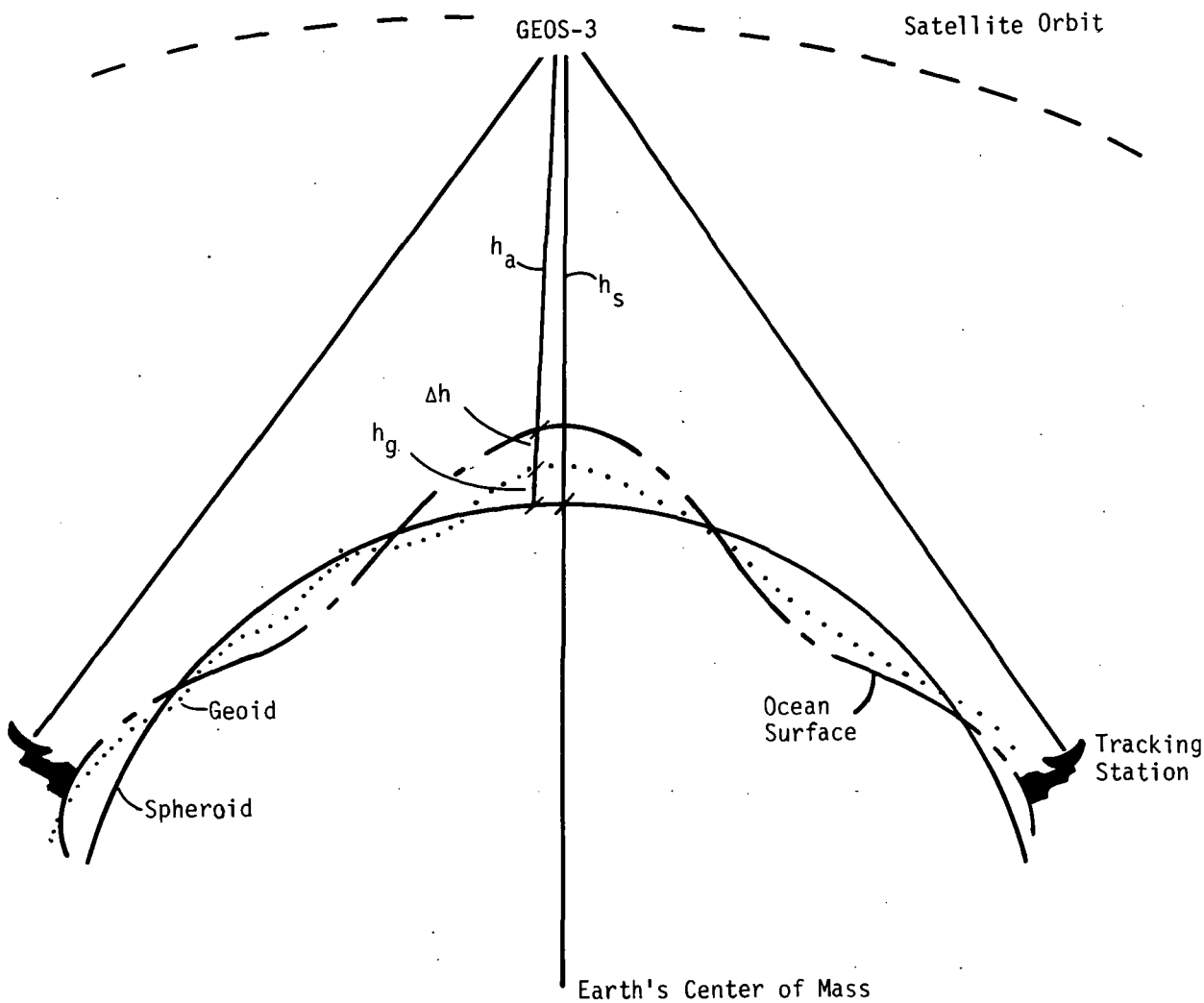

Figure 1. GEOS-3 satellite altimeter geometry. The dynamics effects Δh are obtained by subtracting h_g from the sea surface height $(h_s - h_a)$.

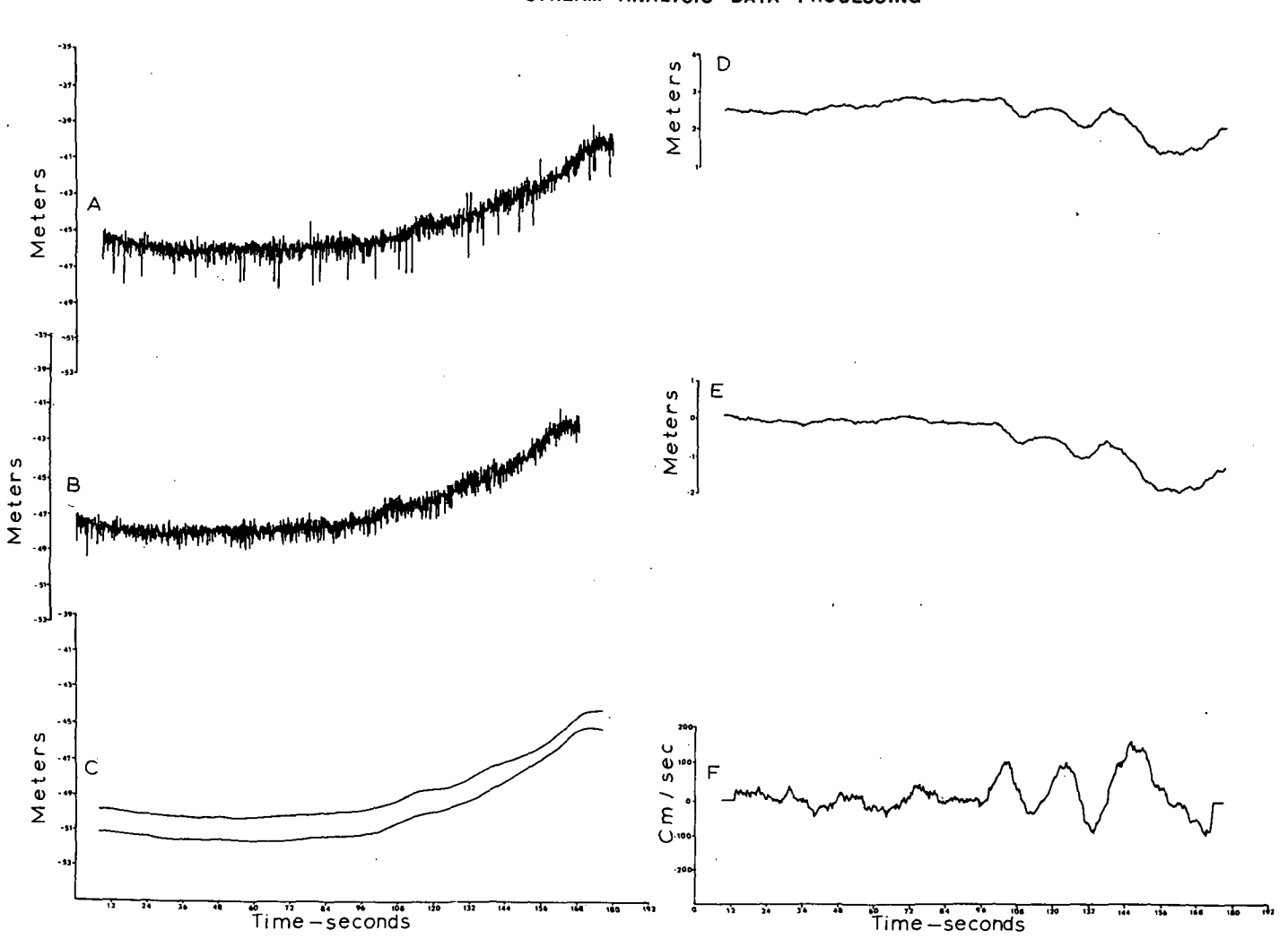

Figure 2. Data processing diagram. The raw sea surface heights (A) are edited (B) and filtered. When compared with the geoid (C) they yield residual values (D) which can be corrected to produce dynamic heights (E). These in turn produce the velocity measurements (F).

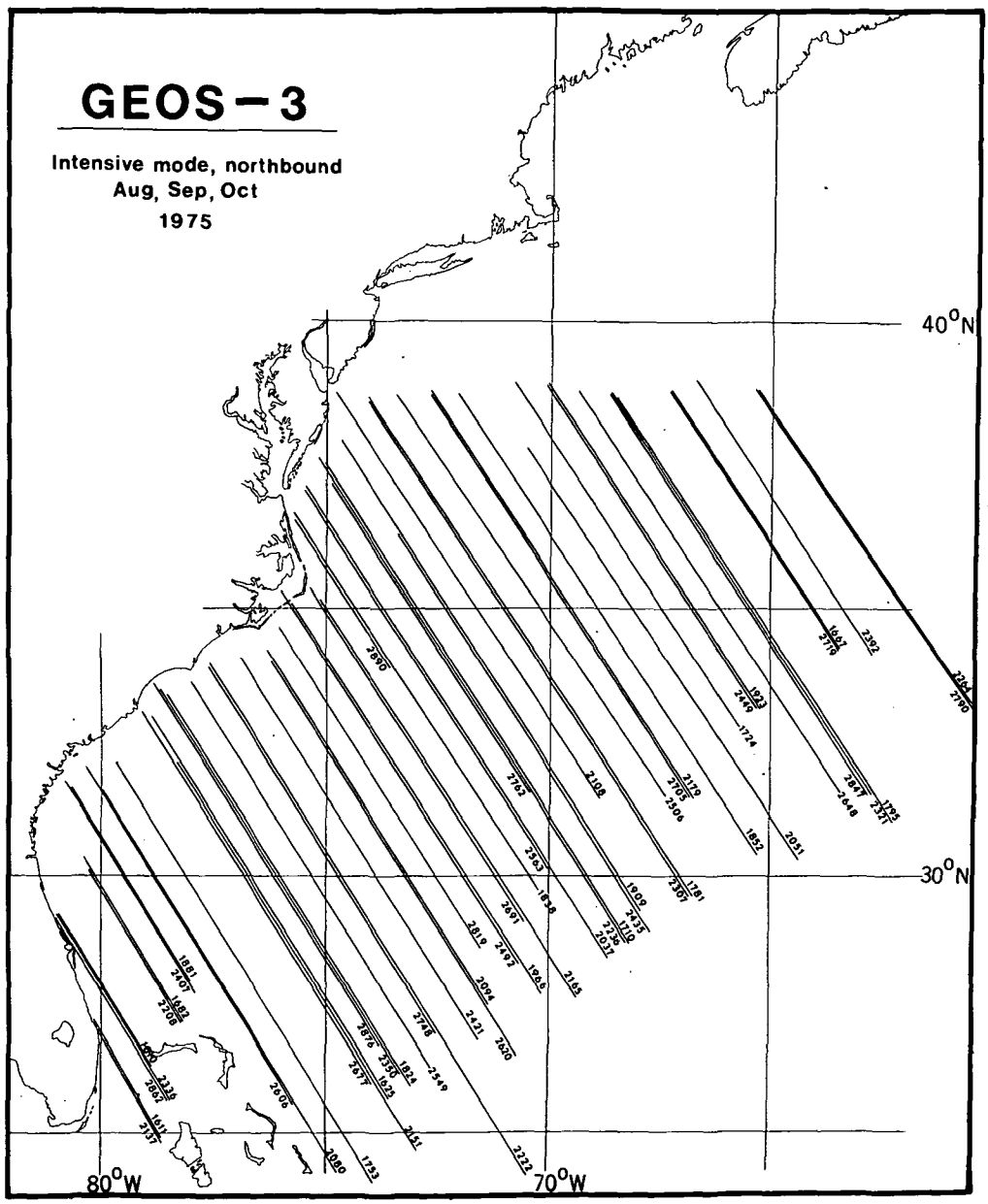

Figure 3. GEOS-3 intensive mode, northbound orbits in August, September, and October 1975, used for this study.

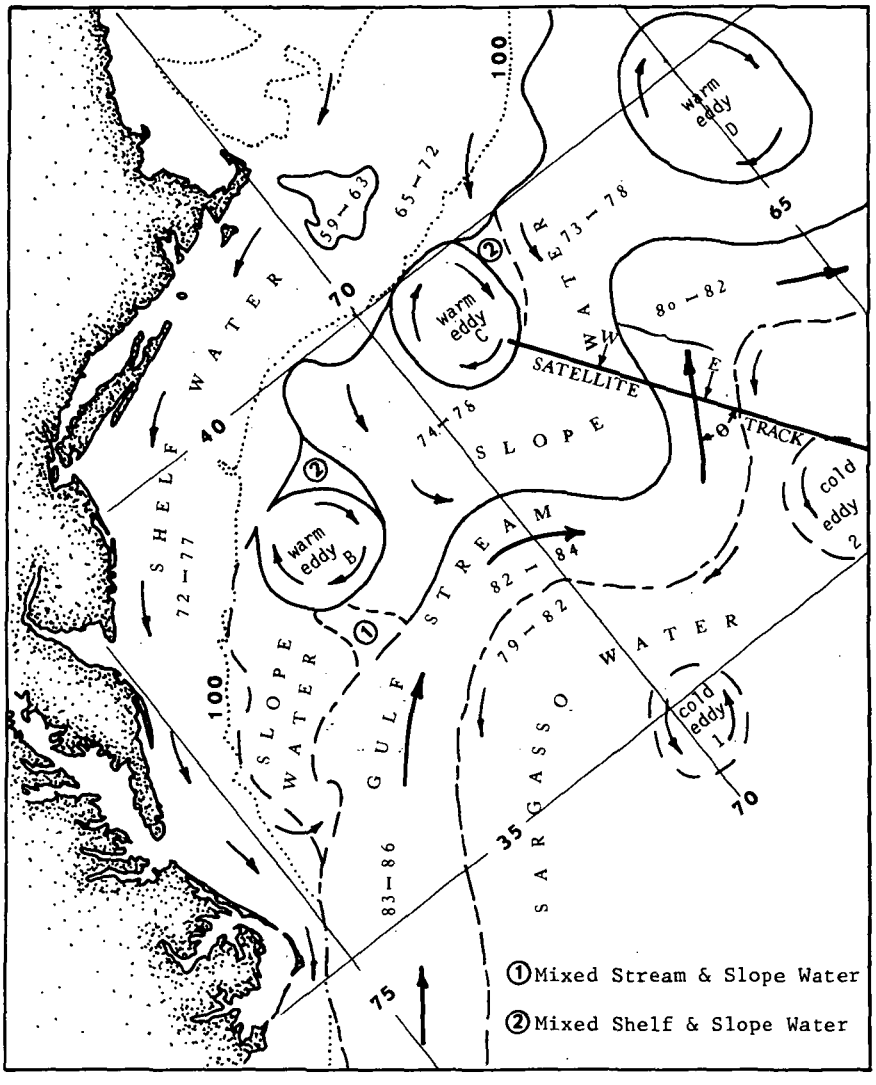

Figure 4. Example of an Experimental Ocean Frontal Analysis (EOFA) chart with subsatellite track for orbit 1795. Water temperatures in °F.

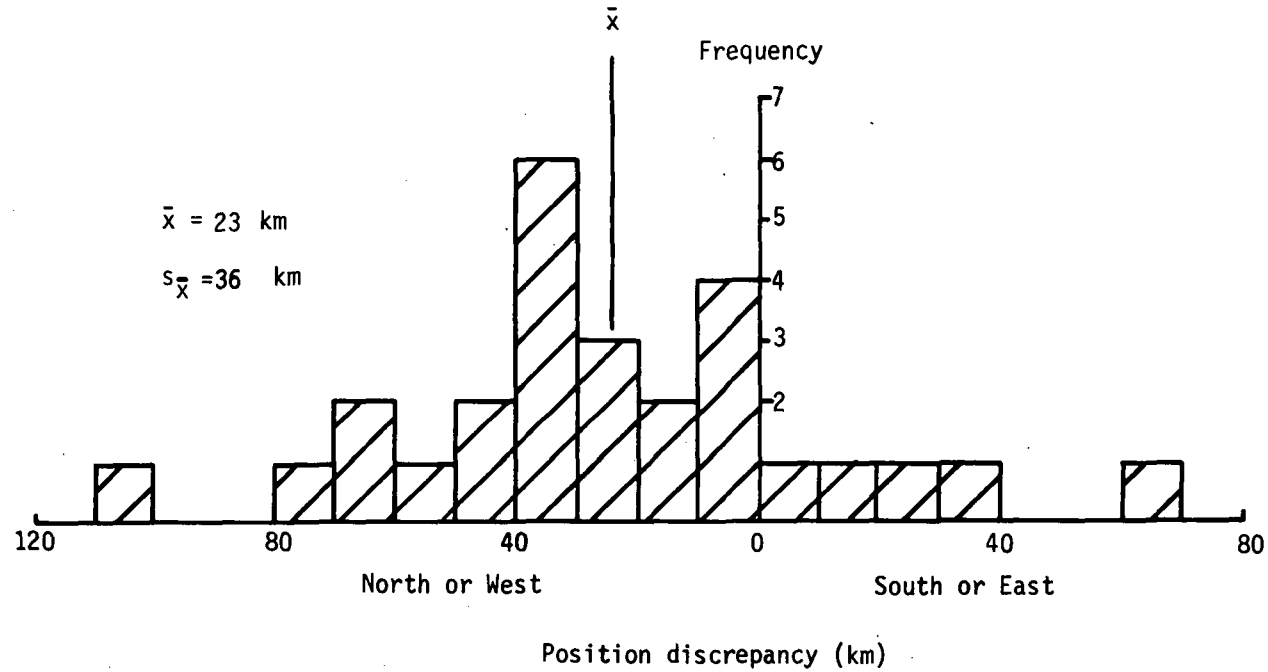

Figure 5. Frequency distribution of the discrepancy in western boundary position as provided by the EOFA charts and GEOS-3 Gulf Stream analysis.

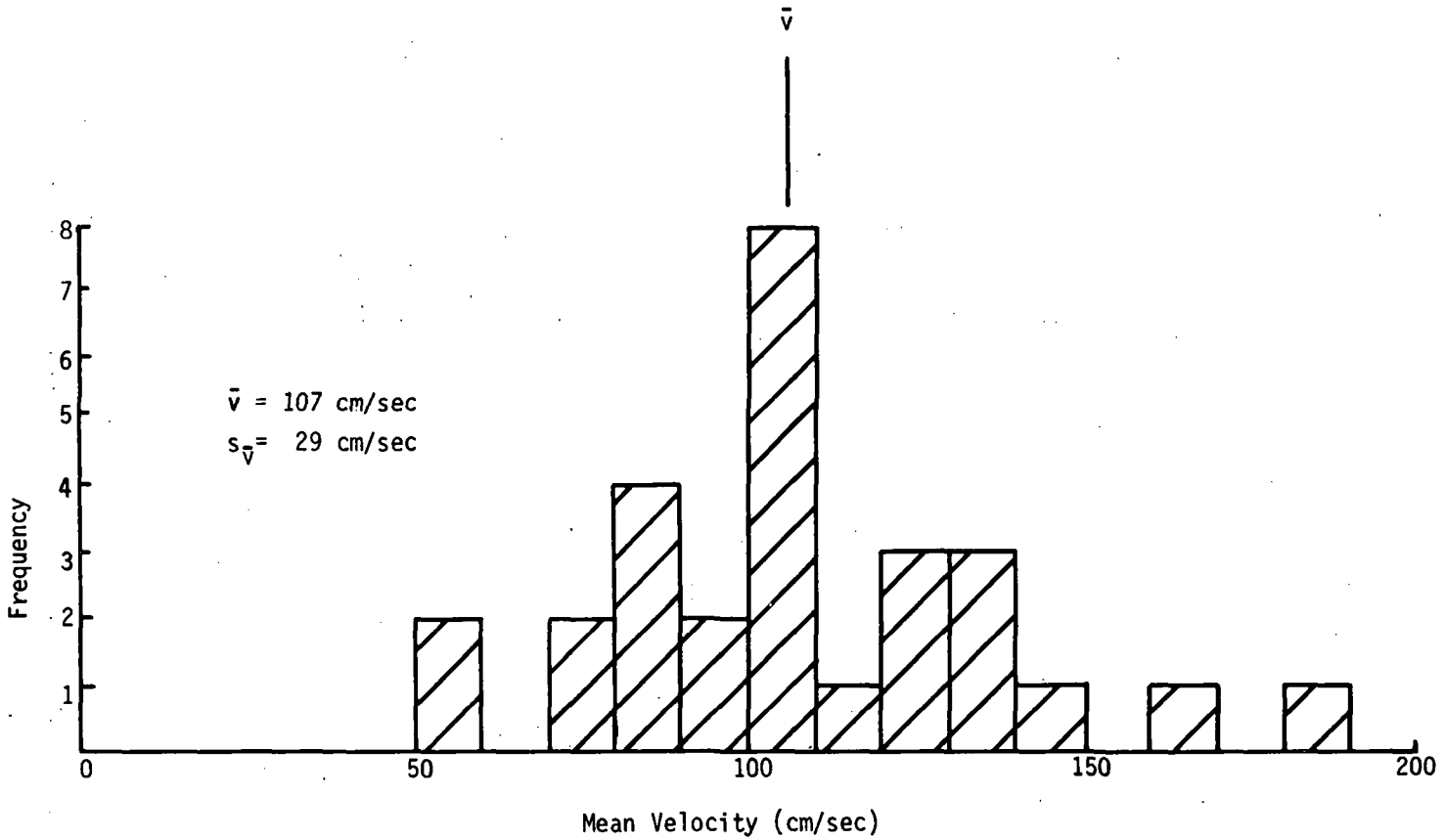

Figure 6. Frequency distribution of the mean velocities as obtained from the GEOS-3 Gulf Stream analysis.

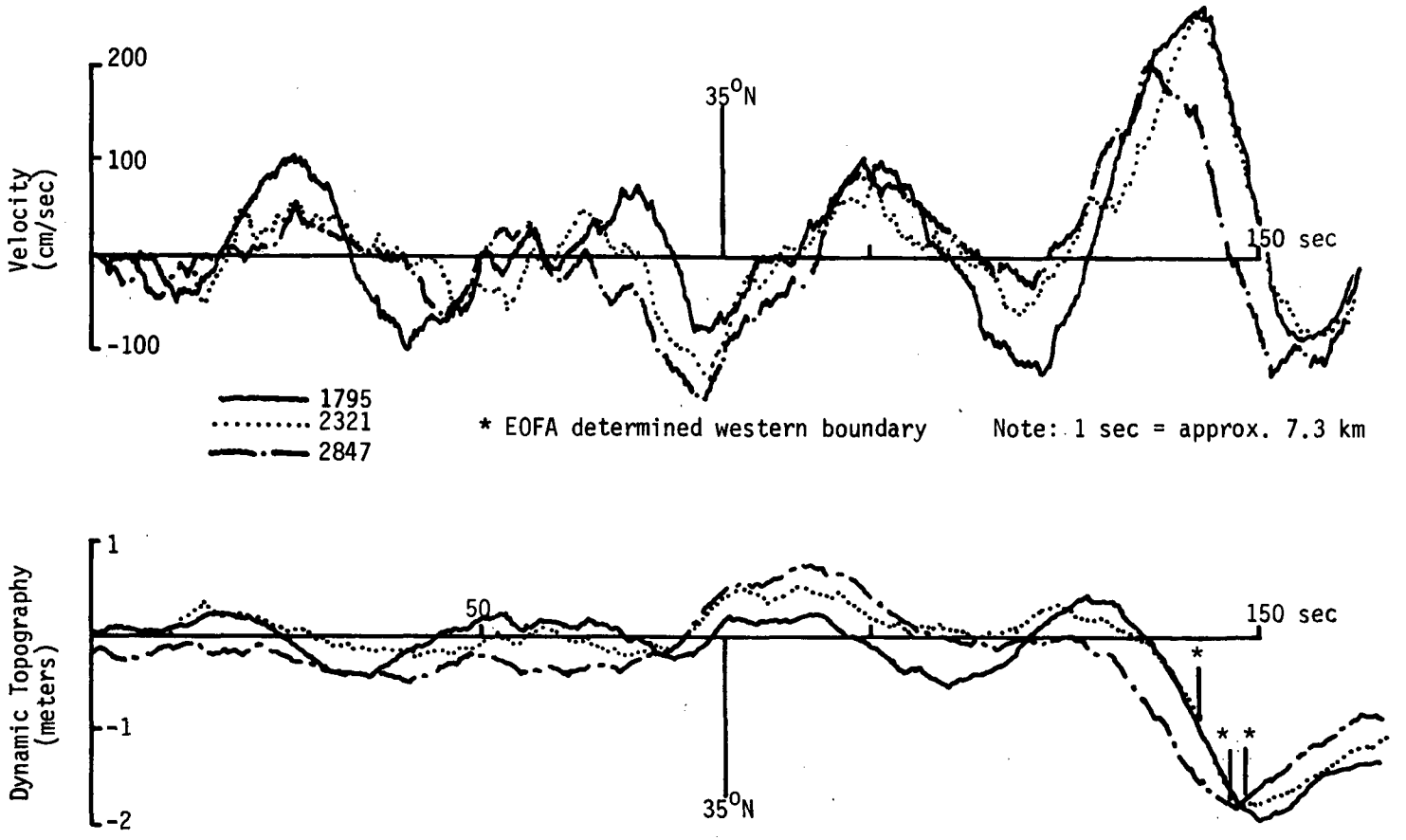

Figure 7. Dynamic heights profile of repeated orbits 1795, 2321, and 2847.

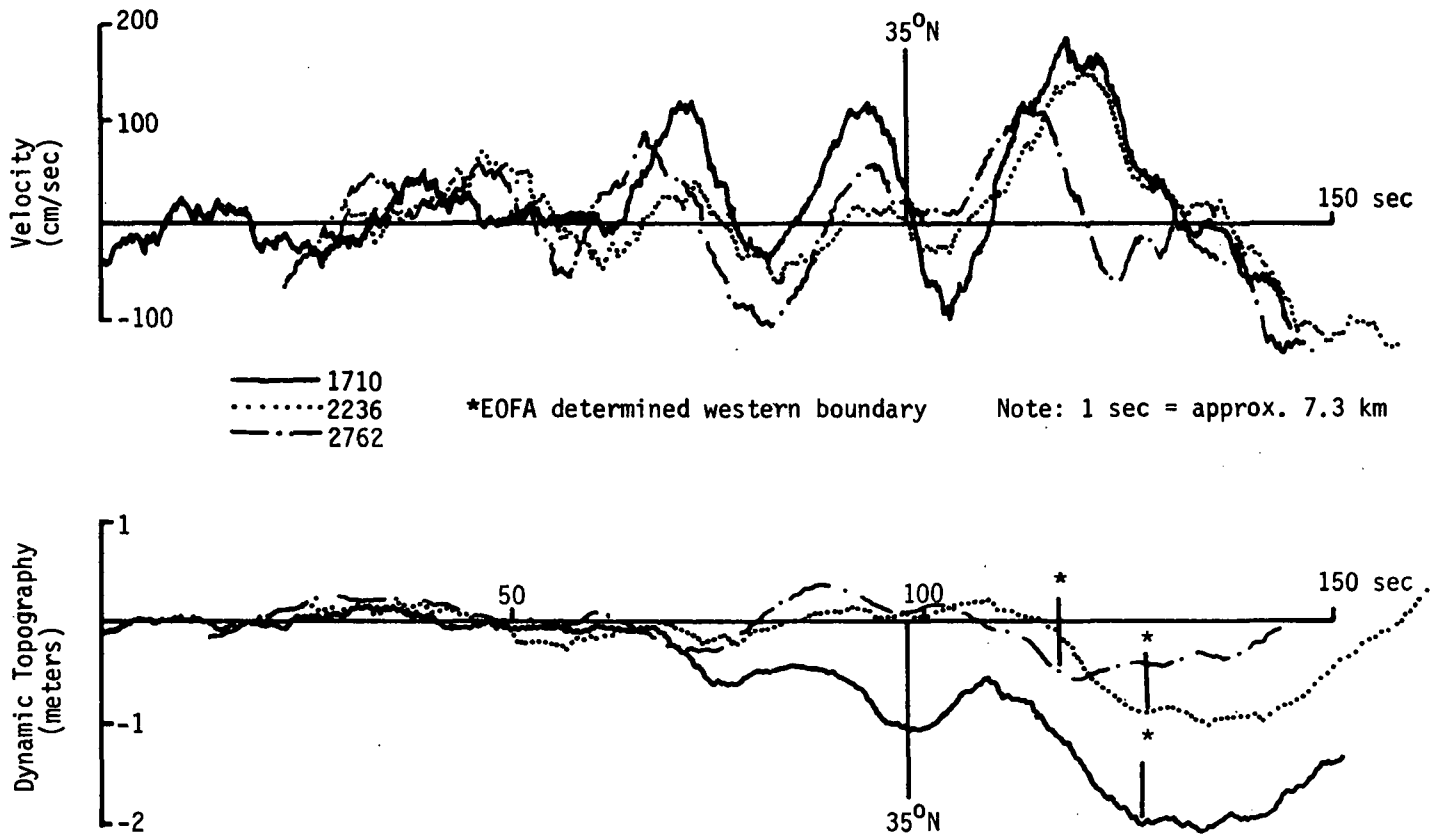

Figure 8. Dynamic heights profile of repeated orbits 1710, 2236, and 2762.

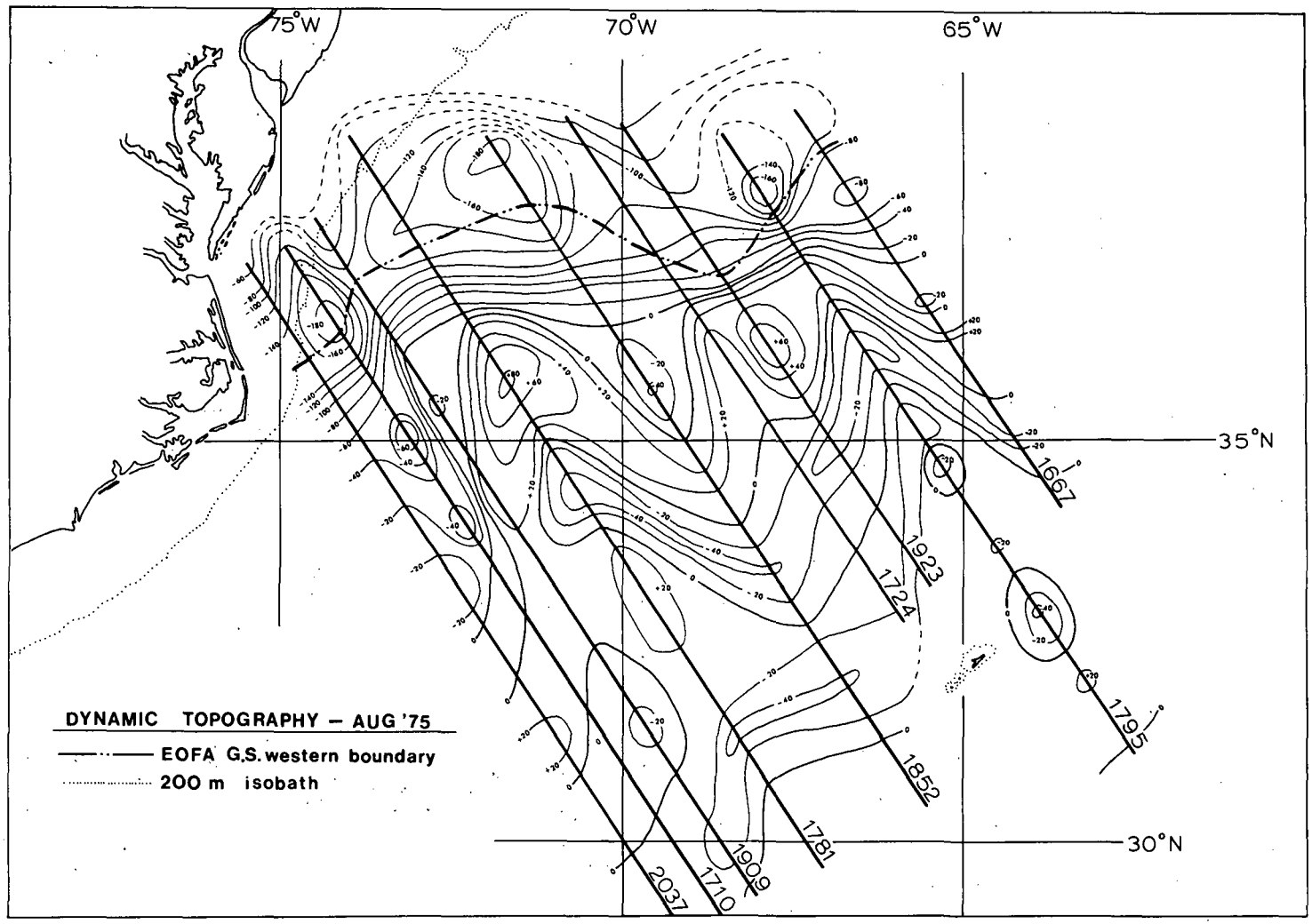

Figure 9. Dynamic topography, August 1975 as obtained from GEOS-3 Gulf Stream analysis of intensive mode, northward passes.

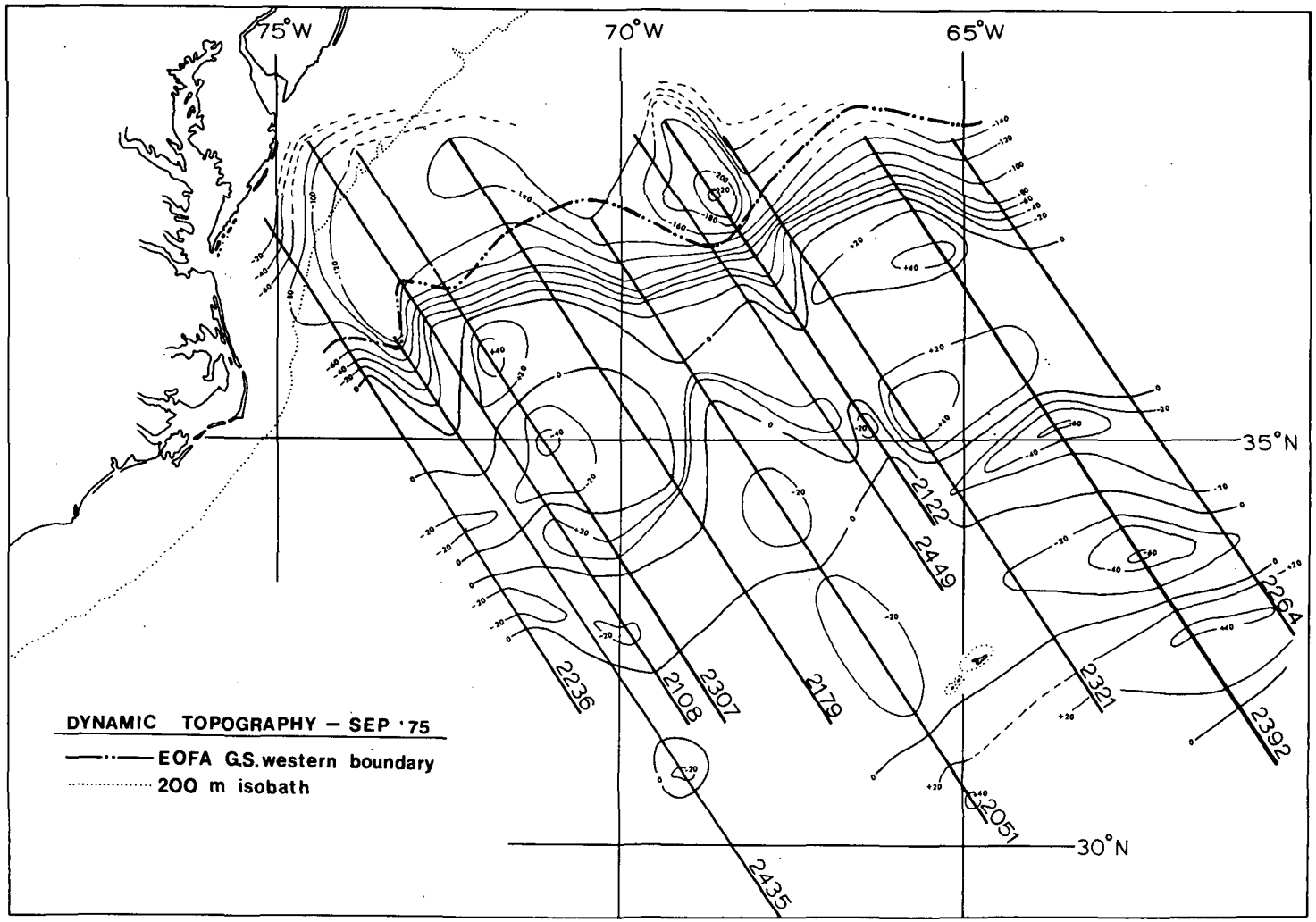

Figure 10. Dynamic topography, September 1975 as obtained from GEOS-3 Gulf Stream analysis of intensive mode, northward passes.

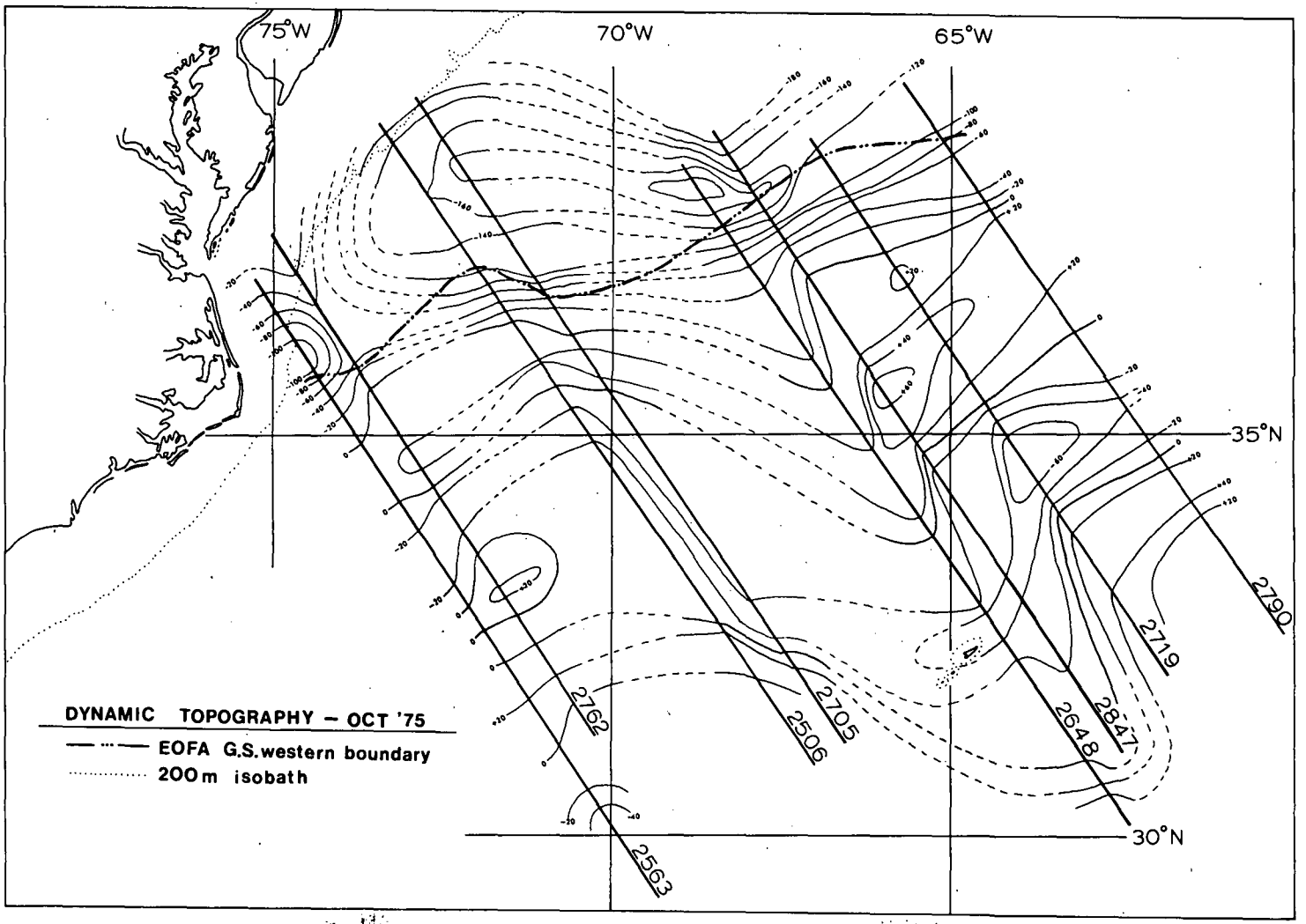

Figure 11. Dynamic topography, October 1975 as obtained from GEOS-3 Gulf Stream analysis of intensive mode, northward passes.

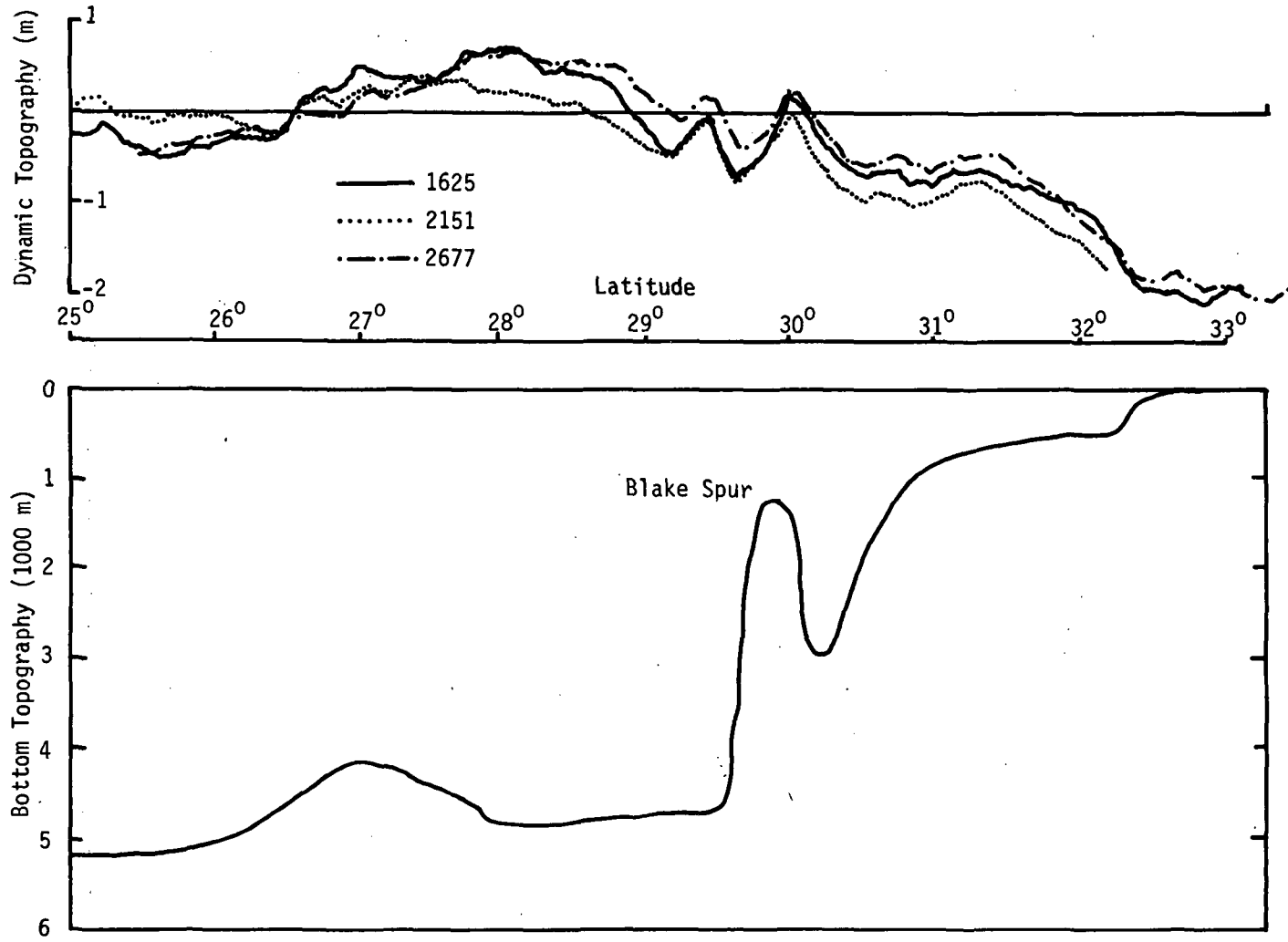

Figure 12. Dynamic heights profile and bottom topography for repeated orbits 1625, 2151, and 2677 depicting geoidal error near the Blake Spur.

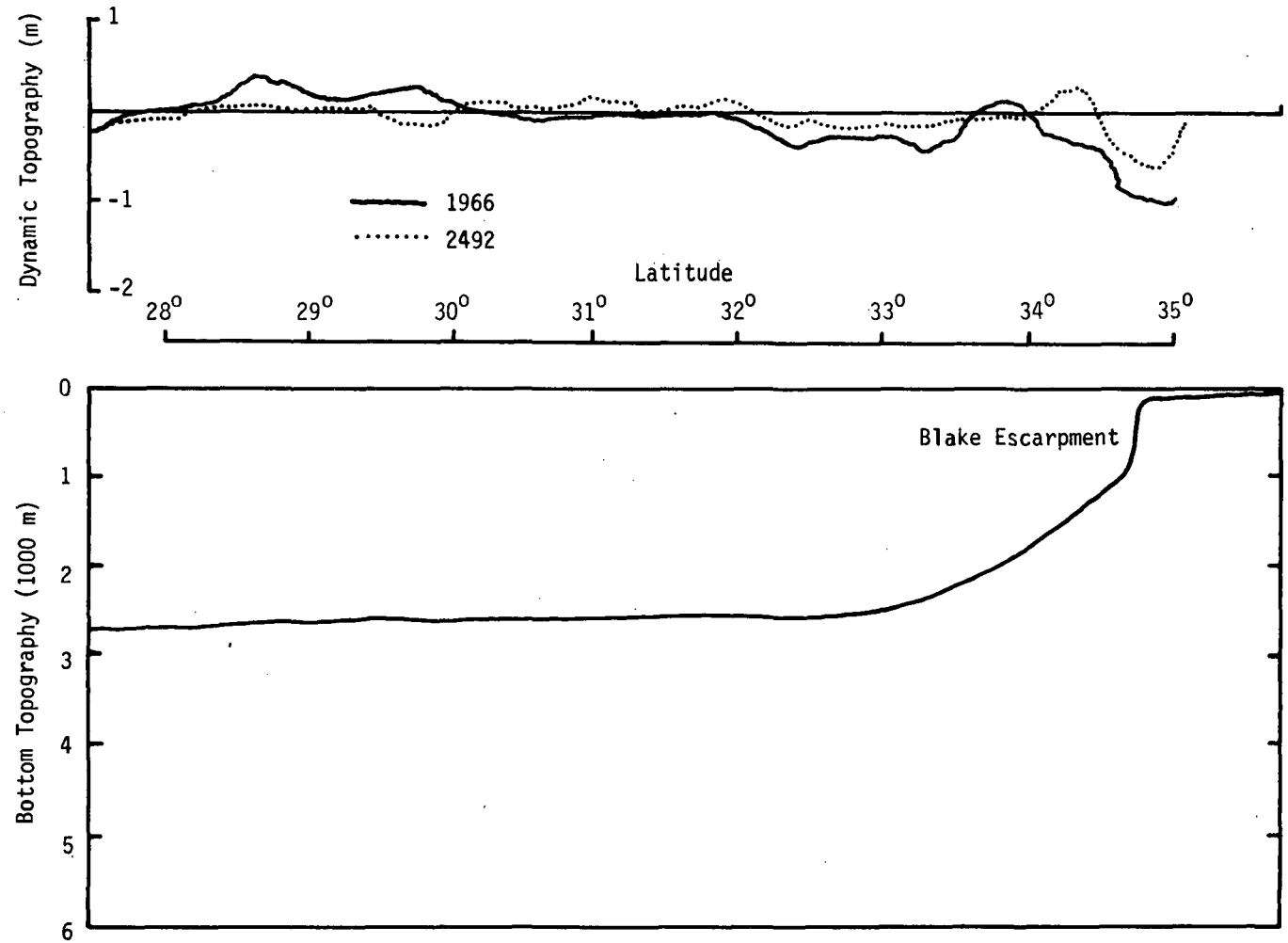

Figure 13. Dynamic heights profile and bottom topography for repeated orbits 1966 and 2492 depicting geoidal error near the Blake Escarpment in the vicinity of Cape Hatteras.

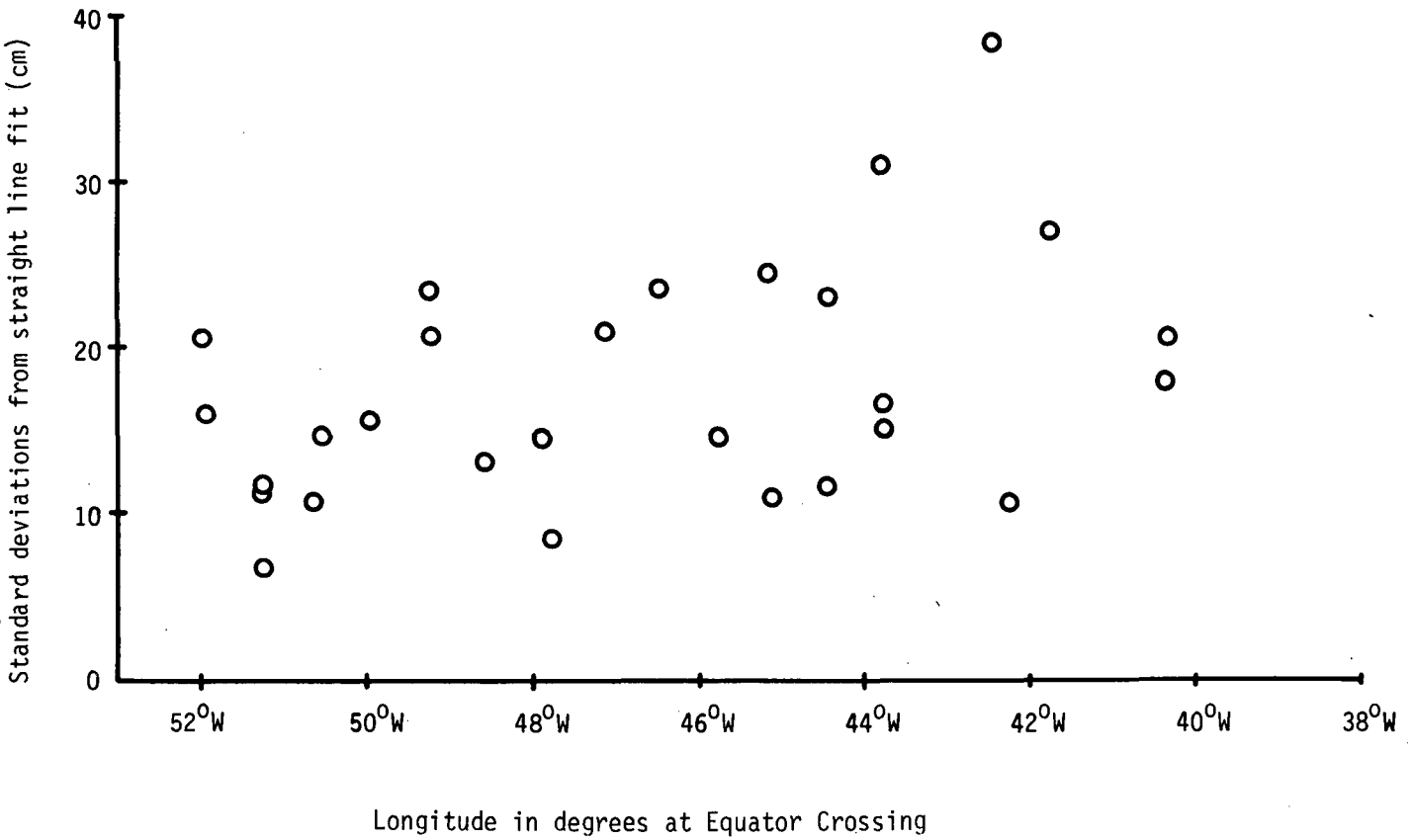

Figure 14. Standard deviations of the dynamic heights over the open ocean plotted against the equatorial crossing, a measure of distance east.

REFERENCES

1. Stommel, H.: The Gulf Stream: A Physical and Dynamical Description, 2nd ed., Berkeley, University of California Press, 1965.
2. von Arx, W. S.: An electromagnetic method for measuring the velocities of ocean currents from a ship under way. Pap. Phys. Oceanogr. and Meteor., 2, 1950, pp. 1-62.
3. Malkus, W. V. R., and M. E. Stern: Determination of ocean transport by electromagnetic effects. J. Marine Res., 11, 1952, pp. 97-105.
4. Rossby, H. T., A. Voorhis, and D. Webb: A quasi-Lagrangian study of mid-ocean variability using long range SOFAR floats. J. Marine Res., 33, 1975, pp. 355-382.
5. Kirwan, Jr., A. D., G. McNally, and J. Coehlo: Gulf Stream kinematics inferred from satellite tracked drifter. J. Phys. Oceanogr., 6, 1976, pp. 750-755.
6. Fofonoff, N. P., and F. Webster: Current measurements in the western Atlantic. Phil. Trans., A 270, 1971, pp. 423-436.
7. Worthington, L. V.: On the North Atlantic Circulation. Baltimore, Johns Hopkins University Press, 1976.
8. Dantzler, Jr., H. L.: Geographic variations in intensity of the North Atlantic and North Pacific oceanic eddy fields. Deep-Sea Res., 23, 1976, pp. 783-794.
9. Fuglister, F. C.: Alternative analysis of current surveys. Deep-Sea Res., 2, 1955, pp. 213-229.
10. Fuglister, F. C.: Gulf Stream '60. Progress in Oceanography. M. Sears, Ed., New York, Pergamon Press, 1963.
11. Warnecke, G., L. J. Allison, L. M. McMillan, and K-H. Szekielda: Remote sensing of ocean currents and sea surface temperature changes derived from the Nimbus II satellite. J. Phys. Oceanogr., 1, 1971, pp. 45-60.
12. Rao, P. K., A. E. Strong, and R. Koffler: Gulf Stream meanders and eddies as seen in satellite infrared imagery. J. Phys. Oceanogr., 1, 1971, pp. 237-239.
13. Strong, A. E., and R. J. DeRycke: Ocean current monitoring employing a new satellite sensing technique. Science, 182, 1973, pp. 482-484.
14. Richardson, P. L., A. E. Strong, and J. A. Knauss: Gulf Stream eddies: recent observations in the western Sargasso Sea. J. Phys. Oceanogr., 3, 1973, pp. 297-301.
15. DeRycke, R. J., and P. K. Rao: Eddies along a Gulf Stream boundary viewed from a very high resolution radiometer. J. Phys. Oceanogr., 3, 1973, pp. 490-492.
16. Legeckis, R.: Applications of synchronous meteorological satellite data to the study of time dependent sea surface temperature changes along the boundary of the Gulf Stream. Geophys. Res. Letters, 2, 1975, pp. 435-438.
17. Stumpf, H. G., and P. K. Rao: Evolution of Gulf Stream eddies as seen in satellite infrared imagery. J. Phys. Oceangr., 5, 1975, pp. 388-393.

18. Voorhis, A. D., D. C. Webb, and R. C. Millard: Current structure and mixing in the shelf/slope water front south of New England. J. Geophys. Res., 81, 1976, pp. 3695-3708.
19. Clark, H. L.: Some problems associated with airborne radiometry of the sea. Appl. Opts., 6, 1967, pp. 2151-2157.
20. LaViolette, P. E., and P. E. Chabot: A method of eliminating cloud interference in satellite studies of sea surface temperatures. Deep-Sea Res., 16, 1969, pp. 539-547.
21. Maul, G. A., and M. Sidran: Atmospheric effects on ocean surface temperature sensing from the NOAA satellite scanning radiometer. J. Geophys. Res., 78, 1973, pp. 1909-1916.
22. McGrath, J. R., and M. F. M. Osborne: Some problems associated with wind drag and infrared images of the sea surface. J. Phys. Oceanogr., 3, 1973, pp. 318-327.
23. Hansen, D. V., and G. A. Maul: A note on the use of sea surface temperature for observing ocean currents. Remote Sens. Environ., 1, 1970, pp. 161-164.
24. Fofonoff, N P.: Dynamics of ocean currents. The Sea, 1, M. N. Hill, Ed., Interscience, 1962.
25. Godbey, T. W.: Oceanographic satellite radar altimetry and wind sea sensor. Oceanography from Space: proceedings. G. C. Ewing, Ed., Woods Hole, Mass., Woods Hole Oceanographic Institute, 1965.
26. Frey, E. J., J. V. Harrington, and W. S. von Arx.: A study of satellite altimetry for geophysical and oceanographic measurements. Proc., 16th International Astronautical Congress, 1966, pp. 53-72.
27. Greenwood, J. A., A. Nathan, G. Neumann, W. J. Pierson, F. C. Jackson, and T. E. Pease: Oceanographic applications of radar altimetry from a spacecraft. Remote Sens. Environ., 1, 1969, pp. 71-80.
28. McGoogan, J. T.: Satellite altimeter applications. IEEE Trans., MTT-23, 1975, pp. 970-978.
29. Heiskanen, W. A., and H. Moritz: Physical Geodesy. San Francisco, W. H. Freeman and Co., 1967.
30. McGoogan, J. T., L. S. Miller, G. S. Brown, and G. S. Hayne: The S-193 radar altimeter experiment. Proc. IEEE, 62, 1974, pp. 793-803.
31. Leitao, C. D. and J. T. McGoogan: Skylab radar altimeter: short wavelength perturbations detected in ocean surface profiles. Science, 186, 1974, pp. 1208-1209.
32. Leitao, C. D., L. S. Miller, and N. E. Huang: Detecting the Gulf Stream using satellite altimetry. Trans. Amer. Geophys. Union, 56, 1974, p. 1107.
33. Hofmeister, E. L., B. N. Keeney, T. W. Godbey, and R. T. Berg: Design error analysis of the GEOS-C radar altimeter. Utica, New York, General Electric Co., Aerospace Electronic Systems Dept., 1975.

34. Geyling, F. T., and H. R. Westerman: Introduction to Orbital Mechanics. Reading, Mass. Addison-Wesley Pub. Co., 1971.
35. Henricksen, S. W., A. Mancini, and B. H. Chovitz, Eds.: The use of artifical satellites for geodesy. Washington, D.C., 3rd International Symposium on the use of artificial satellites for Geodesy, 1972.
36. Marsh, J. G., and S. Vincent: Gravimetric geoid computations and comparisons with Skylab altimeter data in the GEOS-C calibration area. Paper presented at the 16th General Assembly of the I.U.G.G., Grenoble, France, 1975.
37. Marsh, J. G., and E. S. Chang: 5' detailed gravimetric geoid in the northwestern Atlantic Ocean. Marine Geodesy (in press), 1977.
38. Webster, F.: A description of Gulf Stream meanders off Onslow Bay. Deep-Sea Res., 8, 1961, pp. 130-143.
39. Leitao, C. D., C. L. Purdy, and R. L. Brooks: Wallops GEOS-C altimeter preprocessing report. NASA TM X-69357, 1975.
40. Stefansson, U., L. P. Atkinson, and D. F. Bumpers: Hydrographic properties and circulation of the North Carolina shelf and slope waters. Deep-Sea Res., 18, 1971, pp. 383-420.
41. Blanton, J.: Exchange of Gulf Stream water with North Carolina shelf water in Onslow Bay during stratified conditions. Deep-Sea Res., 18, 1971, pp. 167-178.
42. Lee, T. N.: Florida current spin-off eddies. Deep-Sea Res., 22, 1975, pp. 753-765.
43. Semtner, A. J., and Y. Mintz: Numerical simulation of the Gulf Stream and Mid-ocean Eddies. J. Phys. Oceangr., 7, 1977, pp. 208-230.
44. Fuglister, F. C.: Annual variations in current speeds in the Gulf Stream system. J. Marine Res., 10, 1951, pp. 119-127.
45. Hansen, D. V.: Gulf Stream meanders between Cape Hatteras and Grand Banks. Deep-Sea Res., 17, 1970, pp. 495-511.
46. Cheney, R. E., and P. L. Richardson: Observed decay of a cyclonic Gulf Stream ring. Deep-Sea Res., 23, 1976, pp. 143-155.
47. Wyrtki, K., L. Magaard, and J. Hager: Eddy energy in the oceans. J. Geosphys. Res., 81, 1976, pp. 2641-2646.
48. Gould, W. T., W. J. Schmitz, and C. Wunsch: Preliminary field results for a Mid-Ocean Dynamics Experiment (MODE-0) Deep-Sea Res., 21, 1974, pp. 911-931.
49. Gill, A. E., J. S. A. Green, and A. J. Simmons: Energy partition in the large scale ocean circulation and the production of mid-ocean eddies. Deep-Sea Res., 21, 1974, pp. 499-528.
50. Gill, A. E.: Evidence for mid-oceanic eddies in weather ship records. Deep-Sea Res., 22, 1975, pp. 647-652.
51. Sturges, W.: Sea-surface topography near the Gulf Stream. Deep-Sea Res., 15, 1968, pp. 149-156.

52. Robinson, A. R., J. R. Luyten, and F. C. Fuglister: Transient Gulf Stream meandering. Part 1. An observational experiment. J. Phys. Oceanogr., 4, 1974, pp. 237-256.
53. Wilkinson, D. L.: An apparent similarity among ocean eddies. Deep-Sea Res., 19, 1972, pp. 895-898.
54. Warren, B. A.: Topographic influences on the path of the Gulf Stream. Tellus, 15, 1963, pp. 167-183.
55. Johnson, J. A., C. B. Fandry, and L. M. Leslie: On the variation of ocean circulation produced by bottom topography. Tellus, 23, 1971, pp. 113-121.
56. de Szoeke, R. A.: Some effects of bottom topography on baroclinic stability. J. marine Res., 33, 1975, pp. 93-122.
57. Greene, A. H.: Accuracy of satellite radar altimetry measurements. The Use of Artificial Satellites for Geodesy. S. W. Henricksen, A. Mancini, and B. H. Chovitz, Eds., AGU Monograph No. 15, 1972, pp. 227-237.

1. Report No.	2. Government Accession No.	3. Recipient's Catalog No.
NASA TP-1209		

4. Title and Subtitle	5. Report Date
REMOTE SENSING OF GULF STREAM USING GEOS-3 RADAR ALTIMETER	April 1978
	6. Performing Organization Code

7. Author(s)	8. Performing Organization Report No.
C. D. Leitao, N. E. Huang, and C. G. Parra	
	10. Work Unit No.
9. Performing Organization Name and Address	
NASA Wallops Flight Center Wallops Island, VA 23337	11. Contract or Grant No.
	13. Type of Report and Period Covered
12. Sponsoring Agency Name and Address	
National Aeronautics and Space Administration Wallops Flight Center Wallops Island, VA 23337	14. Sponsoring Agency Code

15. Supplementary Notes

16. Abstract

Radar altimeter measurements from the GEOS-3 satellite to the ocean surface indicate the presence of expected geostrophic height differences across the Gulf Stream. Dynamic sea surface heights are found by both editing and filtering the raw sea surface heights and then referencing these processed data to a 5' x 5' geoid. Any trend between the processed data and the geoid is removed by subtracting out a linear fit to the residuals in the open ocean. The inferred mean position of the Gulf Stream's northern (western) boundary is 23 ± 36 km north or west of the Navy's Experimental Ocean Front Analysis mean position, well within the discrepancy of the two methods used. Furthermore, the mean current velocity of 107 ± 29 cm/sec calculated from the dynamic heights for all orbits corresponds rather well with velocities obtained from hydrographic methods. Also, dynamic topographic maps with a 20 cm contour interval for an area 30°-40°N, 60°-75°W are produced for August, September, and October 1975. Results point out limitations in the accuracy of the geoid near Cape Hatteras and the Blake Spur, height anomaly deteriorations due to filtering, and lack of dense time and space distribution of measurements.

17. Key Words (Suggested by Author(s))	18. Distribution Statement
GEOS-3 Altimeter Gulf Stream Ocean Dynamic Topography	Unclassified - unlimited STAR Category - 48

19. Security Classif. (of this report)	20. Security Classif. (of this page)	21. No. of Pages	22. Price*
Unclassified	Unclassified	31	$4.50

* For sale by the National Technical Information Service, Springfield, Virginia 22161

NASA-Langley, 1978

National Aeronautics and Space Administration

Washington, D.C.
20546

Official Business
Penalty for Private Use, $300

SPECIAL FOURTH CLASS MAIL
BOOK

Postage and Fees Paid
National Aeronautics and
Space Administration
NASA-451

U.S. MAIL

NASA

POSTMASTER: If Undeliverable (Section 158 Postal Manual) Do Not Return